

Optical nuclei of radio-loud AGN and the Fanaroff-Riley divide^{*}

P. Kharb and P. Shastri

Indian Institute of Astrophysics, Koramangala, Bangalore – 560 034, India
e-mail: rhea@iiap.res.in

Received 17 June 2003 / Accepted 15 June 2004

Abstract. We investigate the nature of the point-like optical nuclei that have been found in the centres of the host galaxies of a majority of radio galaxies by the *Hubble Space Telescope*. We examine the evidence that these optical nuclei are relativistically beamed, and look for differences in the behaviour of the nuclei found in radio galaxies of the two Fanaroff-Riley types. We also attempt to relate this behaviour to the properties of the optical nuclei in their highly beamed counterparts (the BL Lac objects and radio-loud quasars) as hypothesized by the simple Unified Scheme. Simple model-fitting of the data suggests that the emission may be coming from a non-thermal relativistic jet. It is also suggestive that the contribution from an accretion disk is not significant for the FRI objects and for the narrow-line radio galaxies of FR II type, while it may be significant for the Broad-line objects, and consistent with the idea that the FR II optical nuclei seem to suffer from extinction due to an obscuring torus while the FRI optical nuclei do not. These results are broadly in agreement with the Unified Scheme for radio-loud AGNs.

Key words. galaxies: active – BL Lacertae objects: general – galaxies: nuclei – quasars: general

1. Introduction

The “radio-loud” active galactic nuclei (AGNs) which include radio galaxies, BL Lac objects and quasars, show twin lobes of synchrotron-emitting plasma connected to a “core” by plasma jets on scales of ~ 100 kpc. Fanaroff & Riley (1974) recognised that the radio morphology of radio galaxies along with their total radio power (at 178 MHz) fell into two distinct subclasses: the lower-power Fanaroff-Riley type I (FRI) objects show extended plumes and tails with no distinct termination of the jet while the higher-power type II (FR II) objects show narrow, collimated jets and terminal “hotspots”. The FR II radio galaxies have systematically more luminous optical emission lines (Zirbel & Baum 1995) while FRI radio galaxies inhabit richer environments (Prestage & Peacock 1988); the value of the FRI/FR II radio luminosity break blurs at higher radio frequencies (see Urry & Padovani 1995), and increases with the optical luminosity of the host galaxy (Ledlow & Owen 1996). The origin of the F–R dichotomy is far from clear: suggested possibilities include differences in the spin of the supermassive black hole resulting in different jet kinetic powers (Baum et al. 1995; Meier 1999), galaxy environments (Smith & Heckman 1990), and accretion rates (Baum et al. 1995). The dichotomy issue is complicated by the observations of sources having both FRI and FR II characteristics (FRI/II, e.g., Capetti et al. 1995).

AGN jets experience bulk relativistic motion (Blandford & Konigl 1979) resulting in orientation playing a dominant role

in their appearance and a simple Unified Scheme (US) has emerged (e.g., Urry & Padovani 1995, and refs. therein) according to which the BL Lac objects and radio-loud quasars are the relativistically beamed counterparts of FRI and FR II radio galaxies, respectively. Apart from bulk relativistic motion in radio galaxies, the US requires a ubiquitous optically thick torus in the FR II class of objects (i.e., FR II radio galaxies and radio-loud quasars) which hides the powerful optical continuum and broad emission lines from the nucleus in the edge-on objects, while no such torus is required by the US for the FRI class of objects as broad emission lines are weak/absent, and it has not been clear whether or not a torus exists.

The beamed synchrotron emission from the base of the jet or “core” must extend to visible wavelengths and there is strong evidence for it in BL Lacs and quasars (Impey & Tapia 1990; Wills et al. 1992). Recently, evidence for an optical synchrotron component in the relatively unbeamed radio galaxies has also surfaced, in the form of unresolved nuclear sources in the high resolution images with the *Hubble Space Telescope* (*HST*) (e.g., Chiaberge et al. 1999, 2002; Hardcastle & Worrall 2000; Verdoes Kleijn et al. 2002). These authors argue on the basis of the strong connection with the radio core emission, anisotropy (Capetti & Celotti 1999) and colour information that these optical nuclei are indeed due to synchrotron radiation.

In this paper, we further test the idea that the unresolved nuclear optical emission from radio galaxies is beamed synchrotron emission from the base of the jet, using the radio core prominence parameter (R_c) as an indicator of the orientation of the AGN axes. We then attempt to place these correlations in the broader framework of the US and test for consistencies.

^{*} Appendix C is only available in electronic form at <http://www.edpsciences.org>

We come up with a model-fitting approach to investigate quantitatively the dependence of the optical emission on orientation and further test the predictions of the US in terms of the presence (or absence) of obscuring tori and the contribution of thermal accretion disks. We list the caveats with regard to our current sample and attempt to address them. The outline of the paper is as follows: in Sect. 2 we discuss the optical nuclei in FRI and FR II radio galaxies and the correlations with R_c . In Sect. 3 we compare the optical nuclei with those in BL Lacs and quasars and discuss the results along with model-fitting. The model equations and the fitting procedure are described in Appendices A and B. Section 4 lists the conclusions. Throughout this paper, $H_0 = 75 \text{ km s}^{-1} \text{ Mpc}^{-1}$ and $q_0 = 0.5$ have been adopted and the spectral index α is defined such that $F_\nu = \nu^{-\alpha}$.

2. The optical nuclei in FRI and FR II radio galaxies

Optical nuclei have been detected in a majority of 3CR, B2 and UGC FRI and FR II radio galaxies with the WFPC2 on board the *HST* which appear as unresolved sources with angular sizes $\sim 0''.1$. The results of studies based on this discovery have been presented by Chiaberge et al. (1999); Capetti & Celotti (1999); Hardcastle & Worrall (2000); Capetti et al. (2002); Chiaberge et al. (2002) and Verdoes Kleijn et al. (2002).

For our study, we chose an eclectic sample of FRI and FR II radio galaxies with either such a detected optical nucleus or with an upper limit to its optical flux density from the above-mentioned papers. Our set of FRI radio galaxies comprise 25 3CR (Chiaberge et al. 1999), 17 B2 (Capetti et al. 2002) and 10 UGC FRIs (Verdoes Kleijn et al. 2002) along with NGC 7052 and NGC 6251 from Capetti & Celotti (1999) and Hardcastle & Worrall (1999) respectively. Objects with ambiguous morphologies (e.g., FRI/II sources mentioned in Sect. 1) are excluded. So is 3C 386 whose optical “nucleus” is in fact a foreground star (Chiaberge et al. 2002). We thus have 54 FRI radio galaxies spanning a redshift range of $0.0037 \leq z \leq 0.29$. The FR II radio galaxies include 53 objects from the 3CR sample presented in Chiaberge et al. (2002) and 2 B2 FR IIs from Capetti et al. (2002). Among the 55 FR IIs considered, there are 42 narrow-line radio galaxies (NLRGs) and 13 broad-line radio galaxies (BLRGs). The FR II radio galaxies span a redshift range of $0.025 \leq z \leq 0.296$.

Tables C.1 and C.2 list the FRI and FR II radio galaxies respectively, along with their optical and radio data. Column 1 lists the IAU name; Col. 2: alternative name; Col. 3: redshift (from the references for radio core data, except for UGC FRIs which are from NED); Col. 4: dust disk minor-to-major axis ratio (superscripts “*d*” and “*l*” stand for disk and lane respectively) from Verdoes Kleijn et al. (1999) except 3C 83.1, 3C 296, 3C 449, 3C 465, 3C 326 and 3C 452 which are from de Koff et al. (2000); Col. 5: logarithm of extended radio luminosity at 1.4 GHz in W Hz^{-1} , calculated using the difference between total and core flux density; data at 5 GHz were converted to 1.4 GHz using $\alpha_{\text{radio}}^{\text{ext}} = 0.7$ for extended radio emission; Col. 6: 5 GHz radio core flux density in mJy; Col. 7: reference for the radio core (and total flux density if different); Col. 8: logarithm of radio core prominence standardized to an

emitted wavelength of 6 cm; Col. 9: nuclear optical luminosity in W Hz^{-1} estimated at an emitted wavelength of 5500 Å; Col. 10: reference for nuclear optical flux density/luminosity.

2.1. The correlations with radio core prominence for radio galaxies

The radio core prominence parameter, which is the ratio of the core-to-extended radio flux density ($R_c \equiv S_{\text{core}}/S_{\text{ext}}$) is a known statistical indicator of orientation (Kapahi & Saikia 1982; Orr & Browne 1982) assuming that the core is the unresolved relativistically beamed nuclear jet and the lobes are unbeamed. R_c has indeed been shown to correlate with other orientation-dependent properties both in FR IIs (e.g., Kapahi & Saikia 1982) and FR Is (e.g., Laing et al. 1999). We use the parameter R_c to test if the luminosities of the optical nuclei L_o , are orientation-dependent. If the intrinsic optical synchrotron emission from the jet is relativistically beamed by the Doppler factor δ where $\delta \equiv [\gamma(1 - \beta \cos \theta)]^{-1}$, γ being the Lorentz factor ($\gamma \equiv 1/\sqrt{1 - \beta^2}$), β the bulk velocity in units of the speed of light, and θ being the angle between the radio axis and our line of sight, then L_o should correlate with R_c . We note that L_o has been shown to correlate with the radio core luminosity by Chiaberge et al. (1999); Hardcastle & Worrall (2000).

The optical luminosities of the unresolved *HST* nuclei were K-corrected and calculated at an emitted wavelength of 5500 Å, assuming an optical spectral index $\alpha_{\text{opt}} = 1$. R_c was calculated using observed radio core and total flux densities at 5 GHz and was further K-corrected to an emitted frequency of 5 GHz. For some sources flux densities were estimated from 1.4 GHz assuming $\alpha_{\text{radio}}^{\text{ext}} = 0.7$ and $\alpha_{\text{radio}}^{\text{core}} = 0$ for the extended and core radio emission, respectively. In Fig. 1 we plot L_o versus R_c for the FRI and FR II radio galaxies.

We note that there are many upper limits to L_o . We have analysed the statistical significance of the correlations with the aid of the Astronomical Survival Analysis (ASURV) package as implemented in IRAF, which takes into account data which are only upper/lower limits. L_o turns out to be significantly correlated with R_c for the FRI radio galaxies ($p = 0.0001$, generalized Spearman Rank test, see Table 1), arguing that the nuclear optical emission is orientation-dependent in the same sense as the radio emission and may also originate in the relativistically beamed jet. The implication of the above result is consistent with what Verdoes Kleijn et al. (2002) suggest for their UGC FRI sample, viz., that beaming also plays a role in the variance of L_o , in addition to the intrinsic variance in the nuclear jet $L_{\text{jet}}^{\text{int}}$ which presumably ionizes the line-emitting gas.

For the FR II radio galaxies, the correlation is significant *only if the BLRGs (plotted as stars in Fig. 1) are included*, while the narrow-line objects do not show a significant correlation by themselves ($p > 0.2$, generalized Spearman Rank test). The narrow-line FR II galaxies show no correlation even with the more sensitive parametric Pearson’s correlation test which however uses uncensored data ($p > 0.1$). This lack of correlation could be explained by the presence of a dusty obscuring torus in FR II radio galaxies that is hypothesized by the US;

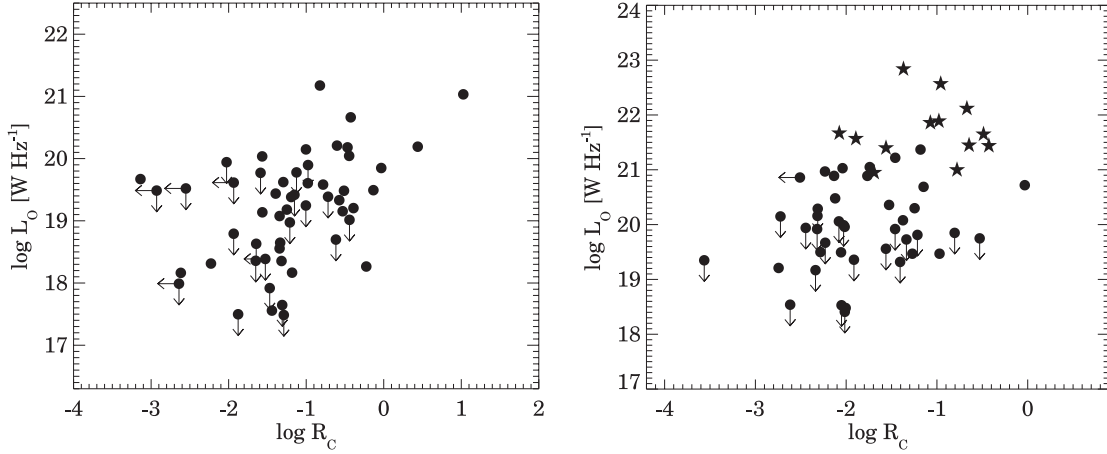


Fig. 1. The luminosity of the optical nuclei L_o , plotted against the radio core prominence R_c , for the FRI (*left*) and FR II radio galaxies (*right*). • radio galaxies, ★ BLRGs, ↓ and ← upper limits. Statistics for the fits are listed in Table 1.

Table 1. Statistics of correlations.

Type	$N (l_x, l_y)$	X	Y	Spearman	Kendall	Schmitt(slope, intercept)
FRI galaxies	54 (5,17)	$\log R_c$	$\log L_o$	0.0001	0.0001	0.52(0.17) 19.40(0.25)
BL Lacs	44 (6,0)	$\log R_c$	$\log L_o$	0.0295	0.0323	0.17(0.14) 22.45(0.16)
FRI and BL Lacs	98 (11,17)	$\log R_c$	$\log L_o$	<0.0001	<0.0001	1.15(0.10) 20.72(0.14)
FRI-BL sample	57 (1,2)	$\log R_c$	$\log L_o$	<0.0001	<0.0001	1.20(0.17) 20.72(0.16)
FR II galaxies	42 (1,20)	$\log R_c$	$\log L_o$	0.2175	0.2392	0.32(0.23) 20.12(0.38)
BLRGs and QSRs	47 (5,0)	$\log R_c$	$\log L_o$	<0.0001	<0.0001	0.60(0.12) 23.15(0.12)
FR II and QSRs	89 (6,20)	$\log R_c$	$\log L_o$	<0.0001	<0.0001	1.18(0.11) 22.26(0.17)
FR II-QS sample	38 (0,3)	$\log R_c$	$\log L_o$	<0.0001	<0.0001	1.12(0.11) 22.71(0.15)
FRI galaxies ^V	9 (0,2)	$b/a (d)$	$\log L_o$	0.2499 ^a	0.2310	1.83(1.22) 17.67(0.89)
"	14 (0,5)	$b/a (d+l)$	$\log L_o$	0.0928 ^a	0.0399	1.91(0.61) 17.54(0.37)
"	9 (0,0)	$b/a (d)$	$\log R_c$	0.0732 ^a	0.0953	-1.09(0.47) -0.19(0.37)
"	14 (0,0)	$b/a (d+l)$	$\log R_c$	0.6065 ^a	0.5200	-0.37(0.40) -0.80(0.23)
FRI galaxies ^D	6 (0,0)	$b/a (d)$	$\log L_o$	0.0845 ^a	0.0909	2.24(0.82) 17.62(0.48)
"	7 (0,0)	$b/a (d+l)$	$\log L_o$	0.0543 ^a	0.0509	2.33(0.76) 17.63(0.54)
"	7* (0,0)	$b/a (d)$	$\log R_c$	0.0802 ^a	0.0985	1.39(0.53) -2.30(0.29)
"	8* (0,0)	$b/a (d+l)$	$\log R_c$	0.0588 ^a	0.0833	1.51(0.48) -2.30(0.29)
FRI galaxies ^{V+D}	12 (0,2)	$b/a (d)$	$\log L_o$	0.1855 ^a	0.1531	1.53(0.70) 17.95(0.44)
"	18 (0,5)	$b/a (d+l)$	$\log L_o$	0.0353 ^a	0.0248	1.90(0.60) 17.66(0.33)
"	12 (0,0)	$b/a (d)$	$\log R_c$	0.7630 ^a	0.6808	-0.06(0.69) -1.06(0.49)
"	18 (0,0)	$b/a (d+l)$	$\log R_c$	0.9085 ^a	0.9698	0.02(0.48) -1.12(0.28)

Statistical significance of various correlations (of X and Y) and linear regression fits. All the results are derived using ASURV as implemented in IRAF. Column 1: the subclass of objects under consideration, “FR II galaxies” refer to narrow-line FR IIs alone, “QSRs” refer to quasars, “FRI-BL” and “FR II-QS samples” refer to the matched subsamples of FR Is and FR IIs as described in Sect. 3.4. FRI galaxies with superscripts V , D , $V+D$ refer to FRI sources from Verdoes Kleijn et al. (1999), de Koff et al. (2000) and from both papers, respectively; ★ an additional FRI source – 3C 430 with a disk of $b/a = 0.15$ and $\log R_c = -2.5$ was included in the $b/a - \log R_c$ correlation; Col. 2: the number of data points and those with limits in X and Y respectively, in paranthesis; Cols. 3 and 4: the independent and dependent variable respectively; b/a being the ratio of the minor-to-major axis of the extended dust feature seen in the *HST* images of radio galaxies, “ d ” and “ l ” standing for a dust disk and a lane respectively, “ $d+l$ ” refers to our jointly considering disks and lanes in the correlations; Cols. 5 and 6: probability that no correlation exists between X and Y from Spearman’s ρ and Kendall’s τ correlation tests respectively; “a” - Spearman Rank test is not accurate as no. of objects, $N < 30$; Col. 7: slope and intercept with standard deviation in parantheses from Schmitt’s linear regression test, bootstrap approximation using 200 iterations, X bins = 10, Y bins = 10.

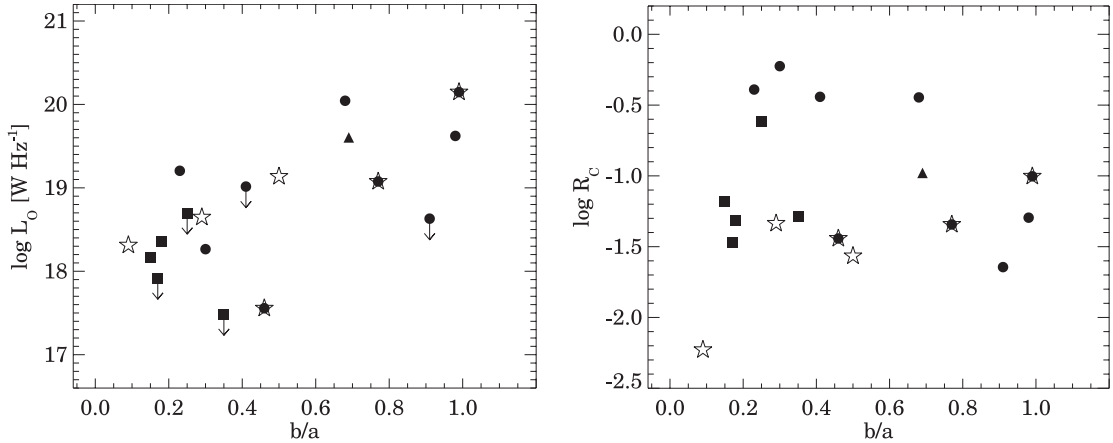


Fig. 2. Nuclear optical luminosity L_o (left) and radio core prominence R_c (right) plotted against minor-to-major axis ratio b/a , for the FRI radio galaxies. \bullet and \blacksquare denote the dust disks and lanes respectively, from Verdoes Kleijn et al. (1999) while the open stars and \blacktriangle denote the dust disks and lanes from de Koff et al. (2000), \downarrow upper limits. The sources common to the two papers are shown by an open star superimposed by \bullet . Table 1 lists the statistics for the correlations.

this could also result in the large number of non-detections (also see Chiaberge et al. 2002).

2.2. Kpc-scale dust disks in FRI radio galaxies

While the evidence for an obscuring torus in FRIs is so far meagre, much larger dust disks and lanes of sizes ~ 100 pc to a few kpc have been discovered in many FRI radio galaxies (e.g., Verdoes Kleijn et al. 1999; de Koff et al. 2000). It has been suggested by Verdoes Kleijn et al. (1999), Capetti & Celotti (1999) and de Koff et al. (2000) that the kpc-scale radio jet tends to align with the axis of this disk. We investigate this point here for the subset of objects where data on dusty disks, as well as L_o and R_c are available. We find different relations of the minor-to-major axis ratio b/a , of the extended dust disk with L_o and R_c for the samples presented in the above papers (see Table 1). b/a of the dust disks correlates significantly both with the L_o and R_c for the de Koff et al. FRI galaxies. b/a correlates significantly with L_o for the Verdoes Kleijn et al. FRI sources *only when both* disks and lanes are considered together. However, they show no correlation with R_c when disks and lanes are taken together, and a correlation in the opposite sense to that predicted, when only disks are considered. When the objects from both samples are combined and both dust disks and lanes are considered, b/a correlates with L_o but not with R_c (see Fig. 2, and Table 1 for the statistical results).

It thus appears that the axes of the extended dust disks do not tend to be aligned with the orientation of the AGN, but that these disks could be causing some extinction of the optical nuclear emission in FRI radio galaxies. This extinction would of course contribute to the scatter in the $L_o - R_c$ correlation.

3. Comparison with the optical nuclei of the beamed objects and the US

In the simple US, the beamed counterparts of the FRI and FRII radio galaxies are the BL Lac objects and the radio-loud quasars respectively. In Sect. 2.1 we find the optical emission

from galaxy nuclei to be orientation-dependent. Given that optical emission from BL Lacs and quasars is also beamed (e.g., Kapahi & Shastri 1987; Baker et al. 1994), we attempt to relate the behaviour of the galaxy nuclei to that of BL Lacs and quasars in the framework of the US. We use this framework to extend the correlations of L_o with R_c to higher values of R_c . We consider the FRI radio galaxies and BL Lacs together (the ‘‘FRI population’’), and similarly consider the FRII radio galaxies and radio-loud quasars together (the ‘‘FRII population’’). To investigate quantitatively the dependence of the optical emission on orientation, we come up with a model-fitting approach. We attempt to apply this to the available data and present the results in Sect. 3.5.1. We further outline the caveats and the drawbacks of our current sample and attempt to address them in Sect. 3.4.

3.1. The data

The set of BL Lac objects we considered comprise both radio-selected and X-ray selected BL Lacs from Perlman & Stocke (1993); Vermeulen & Cohen (1994) and Laurent-Muehleisen et al. (1993), thus including objects having both high and intermediate R_c values. After excluding BL Lacs which showed FRII radio morphology in the form of terminal hotspots viz., 1308+326, 1823+568, 2007+777 (Kollgaard et al. 1992), 1749+701 (O’Dea et al. 1988) and 1803+784 (Cassaro et al. 1999); which were gravitational microlensing candidates, viz., 1413+135 (this object also has other peculiarities like a spiral host galaxy; Perlman & Stocke 1993) and which had uncertain redshifts viz., 0716+714, our BL Lac sample consists of 44 objects spanning a redshift range of $0.028 \leq z \leq 0.997$. We have considered 34 high R_c radio-loud quasars from Vermeulen & Cohen (1994) spanning the redshift range of $0.158 \leq z \leq 2.367$.

We have taken the total optical luminosity of BL Lacs and quasars (as derived from their available V-band magnitudes) as the nuclear optical luminosity, *assuming that the nucleus overwhelms the host galaxy emission*. As the BL Lacs are known

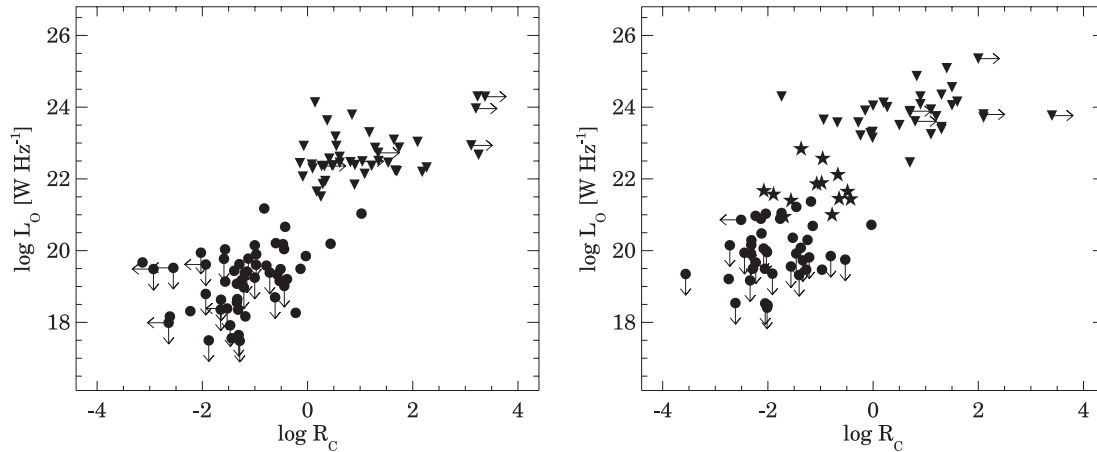


Fig. 3. Nuclear optical luminosity L_o versus radio core prominence R_c for the FRI population (*left*): \bullet radio galaxies, \blacktriangledown BL Lac objects. L_o vs. R_c for the FRII population (*right*): \bullet radio galaxies, \blacktriangledown radio-loud quasars, \star BLRGs. \downarrow and \leftarrow upper limits, \rightarrow lower limits. Statistics for the fits are listed in Table 1.

to be strongly variable, we took radio and optical measurements from the literature that were as closely spaced in time as were available. Several V -magnitudes come from optical monitoring campaigns of Pica et al. (1988); Webb et al. (1988) and Falomo et al. (1994). Quasars can also be optically violent variables (OVVs) but they constitute less than 25% of our quasar sample. The data are tabulated in Tables C.3 and C.4. Column 1 lists the IAU name (B1950); Col. 2: alternative name; Col. 3: redshift (from the references for radio core data, except 1402+042, 0333+321, 0835+580 and 0836+710 which are from Véron-Cetty & Véron (1998)); Col. 4: V -band magnitude; Col. 5: reference for m_i ; Col. 6: logarithm of extended radio luminosity at 1.4 GHz in W Hz^{-1} – taken from the reference for radio core flux density for BL Lacs and calculated using core flux density and radio core prominence for quasars and the BL Lacs 0454+844 and 0735+178; data at 5 GHz converted to 1.4 GHz using $\alpha_{\text{radio}}^{\text{ext}} = 0.7$ for the extended radio emission; Col. 7: 5 GHz radio core flux density in mJy; Col. 8: reference for the radio core and total flux density (for quasars it is the reference for the radio core flux density and $\log R_c$); Col. 9: logarithm of radio core prominence standardized to an emitted wavelength of 6 cm; Col. 10: nuclear optical luminosity in W Hz^{-1} estimated at an emitted wavelength of 5500 Å. The plots of L_o against R_c for the FRI and FRII populations are shown in Fig. 3.

3.2. Caveats

While interpreting the $L_o - R_c$ plots, it is important to keep the following caveats in mind.

1. The objects constitute an *eclectic* sample, with no rigorous selection criteria applied.
2. The beamed and unbeamed objects are not matched in redshift, nor in extended radio luminosity. We discuss the significance of this in Sect. 3.3 and try to define a “matched” sample in Sect. 3.4.
3. The L_o values for the BL Lacs and quasars are derived from their total magnitudes, and include the host galaxy contribution. Particularly in the intermediate R_c regime for BL Lacs,

the host galaxies could contribute significantly to the assumed nuclear optical luminosity.

We address some of these issues later in the paper.

3.3. Correlations with radio core prominence for the two populations

For both the FR populations, the $L_o - R_c$ correlation *does* extend to higher R_c , broadly consistent with the predictions of the US and again reinforcing the idea that the optical nuclear emission is orientation-dependent in the same way as the radio core emission and it may thus constitute the optical counterpart of the relativistically beamed radio synchrotron jet. Using survival analysis, the generalized Spearman’s Rank correlation test indicates that the FRI and FRII populations both show a significant correlation ($p < 0.0001$) of L_o with R_c (see Table 1).

For the FRII population, we showed in Sect. 2.1 that the narrow-line FRIIs do not show any correlation by themselves. A significant correlation ($p < 0.0001$, generalized Spearman Rank test) exists for the broad-line objects, however, i.e., for the the broad-line radio galaxies and quasars. These two observations taken together are consistent with there being obscuration effects by a torus in the FRIIs. Also, though fewer FRIIs than FRIIs show detected optical nuclei, optical nuclei have been detected in *all* the BLRGs observed (where the US predicts no obscuration by the torus), again consistent with this idea. Chiaberge et al. (2000) also suggest obscuration effects on the basis of the non-detection of optical nuclei in some narrow-line FRIIs.

The BL Lacs by themselves also show a significant correlation of L_o with R_c , but the plot is flatter than what is expected from beaming alone. This could be due to the fact that their L_o values include the contribution from the host galaxy, particularly since this contamination is likely to be more severe at intermediate values of R_c . Although for many BL Lac objects where host galaxies have been imaged (e.g., Jannuzi et al. 1997) the difference between the nuclear and the total optical luminosity (L_o) is less than the 50% errors assumed in L_o (e.g., Verdoes Kleijn et al. 2002, see Appendix B) for

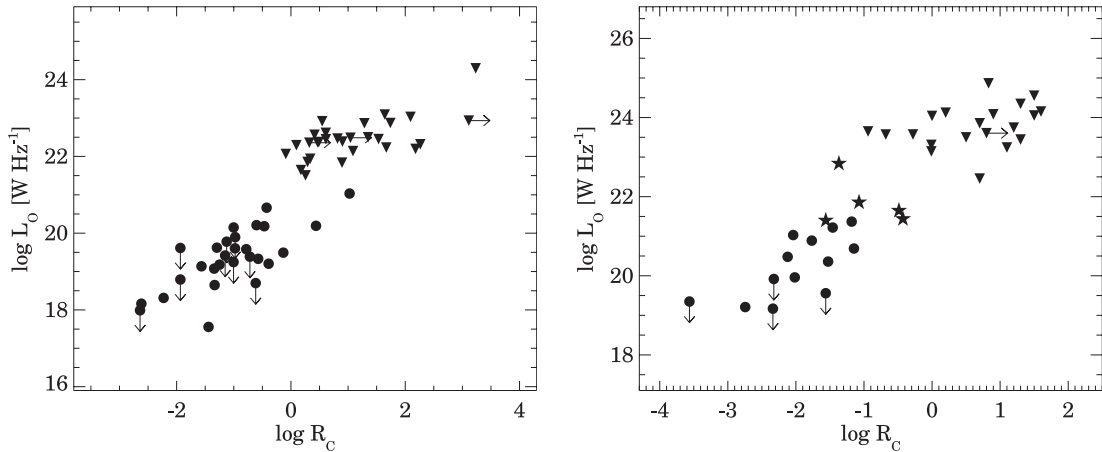


Fig. 4. Nuclear optical luminosity L_o versus radio core prominence R_c for the matched subsample of FRI galaxies and BL Lac objects (*left*) and FR II galaxies and quasars (*right*). • radio galaxies, ▾ BL Lac objects (*left*) and quasars (*right*), ★ BLRGs, ↓ upper limits, → lower limits. Statistics for the fits are listed in Table 1.

some sources this difference can as high as a magnitude (e.g., Kotilainen et al. 1998). In principle, the flattening could also be due to the presence of a luminous accretion disk, in which case the BL Lacs cannot be considered to be consistent with the unbeamed FRI radio galaxies. The use of nuclear luminosities uncontaminated by host galaxy emission for *all* the objects would clarify the issue. We are in the process of investigating this point which is part of a future paper.

A two-dimensional Kolmogorov-Smirnov test shows that the FRI and FR II populations are different at the $p < 0.0001$ level. For each of the populations, a multiple linear regression test using the statistics packages STATISTICA and ASURV (the “Buckley James” algorithm) of R_c , redshift (z) and extended radio luminosity (L_{ext}) as independent variables, shows that the correlation coefficient for the $L_o - R_c$ correlation is the most significant ($p < 0.0001$). L_{ext} is the next most significant contributor. Since L_{ext} can reasonably be assumed to be an indicator of intrinsic AGN power, this implies that variation in intrinsic nuclear power contributes significantly to the scatter in the $L_o - R_c$ correlation. As expected, the nuclear optical luminosity is correlated with redshift, both because luminosity is expected to correlate with redshift, and because of the absence of high redshift radio galaxies in the samples.

3.4. Matched subsamples of FRI and FR II objects

Ideally, all the objects in each population ought to be intrinsically similar in the framework of the US, which means that they should all be of similar intrinsic power, from the same volume of space, and with a narrow distribution of other orientation-independent parameters. As a next best step, we attempt here to derive a “matched” sample for the two FR populations, keeping in mind the multiple linear regression results for the whole sample discussed in the previous section.

For the FRI matched subsample, we restrict the redshifts to $z < 0.3$ and the extended radio luminosity at 1.4 GHz to $23.5 \leq \log L_{\text{ext}} \leq 25 \text{ W Hz}^{-1}$. For the FR II matched subsample, the redshifts are constrained to $z < 1.3$, while the

extended radio luminosity is $26.2 \leq \log L_{\text{ext}} \leq 27.6 \text{ W Hz}^{-1}$. Figure 4 shows the $L_o - R_c$ correlations for these subsamples while the correlation and regression parameters are listed in Table 1. We find that the scatter seen in Fig. 3 is considerably reduced in Fig. 4 and the correlations improve significantly compared to the unrestricted samples. Multiple linear regression tests on the restricted samples with the independent variables, R_c , z , L_{ext} show that the $L_o - R_c$ is still the strongest correlation ($p < 0.0001$) while the contribution of L_{ext} is no longer significant.

3.5. Model-fitting the $L_o - R_c$ data

If bulk relativistic motion with a single Lorentz factor (γ) value applicable to the whole population were alone responsible for the variation in L_o , then the logarithmic plot of L_o against R_c would be linear. Any additional factors such as orientation effects due to a torus or thin thermal disk will cause this relationship to deviate from linearity. We attempt to fit some simple models to the data along these lines. Appendix A gives the model equations while Appendix B describes the different models considered along with the model-fitting procedure.

We assume that the nuclear optical luminosity L_o is, in the most general case, due to the sum of synchrotron emission from the base of a relativistic jet, and thermal emission from a thin accretion disk, modified by the presence of an optically thick torus. Keeping in mind that we are only attempting to explore the potential of such a model-fitting approach and that our sample is not rigorously selected, we consider this simple model here and do not include the possibility of variation in *intrinsic* nuclear power as discussed in Sect. 3.3, nor the possibility of extinction of the optical nucleus by an extended kpc-scale dusty disk which was discussed in Sect. 2.2. Our models also do not take into account any intrinsic spread in the Lorentz factors, nor the possibility that the relevant Lorentz factor for the highly beamed and mildly beamed subclasses may be systematically different due to a “spine-sheath” type structure of the jet (e.g., Hardcastle et al. 1996; Laing et al. 1999). However, as the multiple linear regression tests discussed in Sect. 3.3

Table 2. Parameters from the different model-fits for the FR populations.

	Model	A_{V_0}	θ_c	Model		Outputs		AIC
				$L_{\text{jet}}^{\text{int}}$	σ	L_{disk}	σ	
FRI	Jet only	2.7e+20	1.3e+19	295.2
	Jet+Disk	2.6e+20	1.4e+19	8.5e+17	1.1e+18	297.1
	Jet+Disk+Torus	3.0	45	2.7e+20	1.5e+19	3.5e+18	1.6e+18	304.5
	Jet+Torus	3.0	45	2.9e+20	1.4e+19	303.1
	Best fit	0.1	90	2.6e+20	1.3e+19	295.3
Matched FRI	Jet only	3.8e+20	2.5e+19	132.3
	Jet+Disk	4.1e+20	2.9e+19	-7.9e+18	2.0e+18	133.4
	Jet+Disk+Torus	3.0	45	4.4e+20	3.3e+19	-1.4e+18	4.1e+18	137.0
	Jet+Torus	3.0	45	4.4e+20	2.9e+19	135.0
FR II	Jet only	5.8e+21	3.0e+20	269.6
	Jet+Disk	6.5e+21	3.7e+20	-6.7e+19	1.2e+19	270.7
	Jet+Disk+Torus	3.0	45	6.7e+21	3.9e+20	-5.8e+19	1.5e+19	272.9
	Jet+Torus	3.0	45	6.1e+21	3.2e+20	271.5
	Best fit	3.0	37	6.5e+21	3.4e+20	270.8
Matched FR II	Jet only	1.6e+21	1.3e+20	94.3
	Jet+Disk	1.8e+21	1.5e+20	-1.9e+20	2.1e+19	93.4
	Jet+Disk+Torus	3.0	45	2.0e+21	1.7e+20	-2.1e+20	2.5e+19	95.9
	Jet+Torus	3.0	45	1.8e+21	1.4e+20	96.2
BL FR II	Jet only	2.2e+22	1.6e+21	127.3
	Jet+Disk	1.3e+22	1.2e+21	1.5e+22	2.7e+21	123.3
BL Lacs*	Jet only	1.2e+21	9.0e+19	118.4
	Jet+Disk	6.2e+19	1.4e+19	3.3e+22	3.0e+21	78.6

★ See Sect. 3.5.1 in the text. In Col. 1 FRI/FR II and Matched FRI/FR II stand for the FRI/FR II population and its matched subsample as discussed in Sect. 3.4, BL FR II stand for the broad-line FR IIs viz., BLRGs and quasars. A_{V_0} and θ_c (in degrees) are the fixed initial parameters for the models where a torus is incorporated. σ is the standard deviation for the variable on the left. A lower AIC (Akaike’s Information Criterion) value indicates a better model fit. The “Best fit” model is the “Jet+Torus” model for FR Is and FR IIs for which AIC is lowest (see Appendix B and Sect. 3.5.1), the A_{V_0} and θ_c (in degrees) are the parameters corresponding to this fit.

suggest, orientation appears to play the most dominant role in the variation of L_o . To quantify the goodness-of-fit of a particular model, we have used Akaike’s information criterion (AIC). The AIC (Akaike 1974) is a likelihood criterion with an added penalty term corresponding to the complexity of the model, and measures the trade-off between model complexity/parsimony and goodness-of-fit. Smaller AIC values indicate a better fit. Appendix B describes the usage of AIC to derive the best model-fits to the FRI and FR II data.

3.5.1. The results

The results of the model-fitting are given in Table 2. For the FRI population, the “Jet-only” model is better than all the others. The “Jet+Disk” model in fact yields a value for the accretion disk luminosity L_{disk} , which is comparable to its standard deviation σ obtained from the fitting. Further, the “Jet+Torus” model is best fitted by the torus extinction parameter $A_{V_0} \approx 0.1$ and half-opening angle $\theta_c \approx 90^\circ$, which are

equivalent to there being no torus. We note here that, based on the high rate of detections of optical nuclei in FR Is, Chiaberge et al. (1999) have also suggested that there is no obscuring torus in them. Further, Perlman et al. (2001) have failed to detect thermal emission from a dusty torus in the 10 μm image of the nearby FRI radio galaxy, M 87.

For the FR II population as a whole, the results are less clear. Formally, the “Jet-only” model has the lowest AIC value, but the other models also yield comparable values. However, the L_{disk} that is obtained for “Jet+Disk” and “Jet+Disk+Torus” is unphysical. When only the broad-line objects among the FR IIs, viz., the BLRGs and quasars are considered, the “Jet+Disk” model was a better fit than the “Jet-only” model (Table 2). This is consistent with the fact that the “big blue bump” (attributed to the accretion disk) is observed in all these objects, and, in the framework of the US, their central regions are not obscured by the torus. For the whole population, a larger number of data points in the regime where the disk is expected to be relatively most prominent, viz., the intermediate

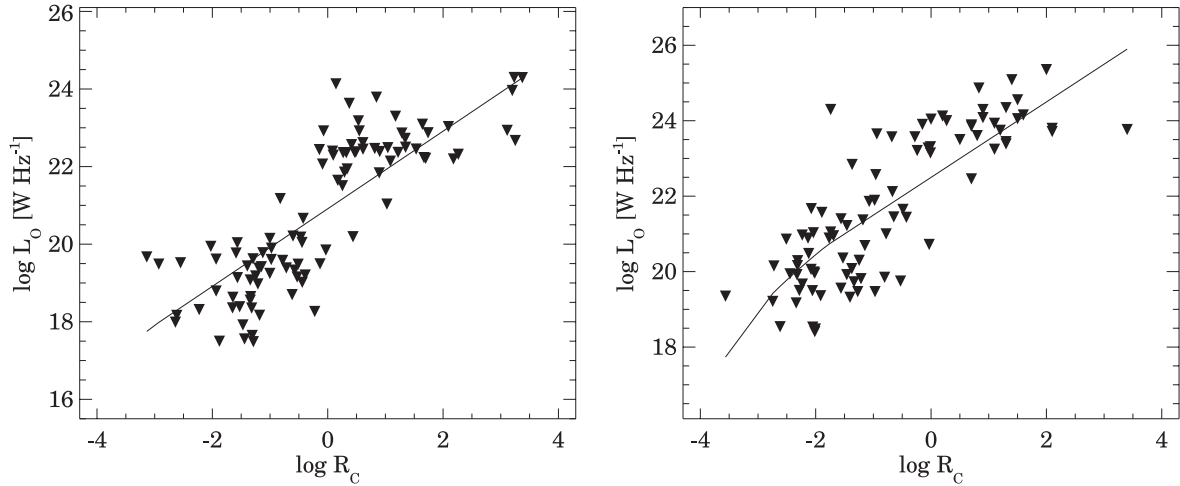


Fig. 5. Best fits to the FRI (*left*) and FRII (*right*) populations using only a “Jet+Torus” model. Table 2 lists the model parameters.

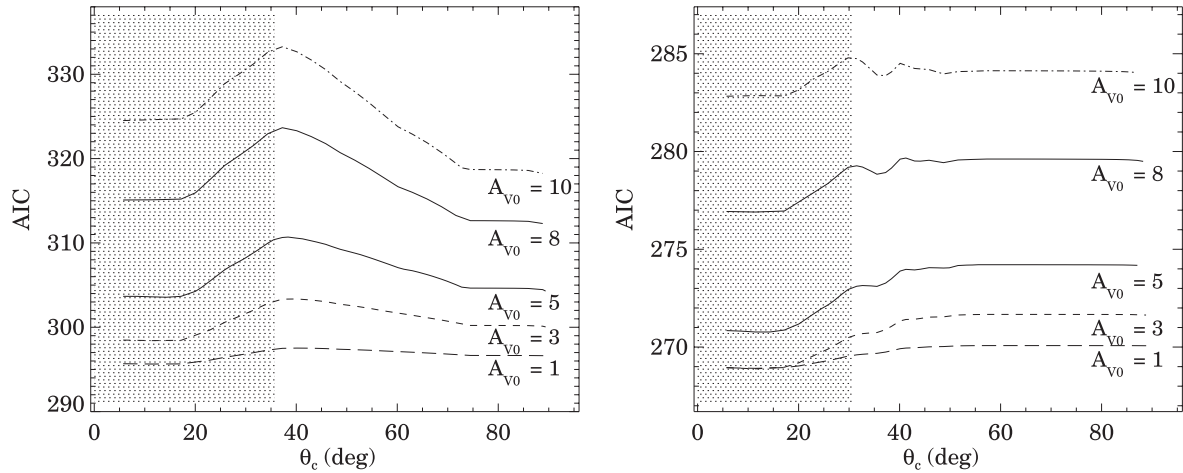


Fig. 6. AIC values for different initial A_{V_0} plotted against torus opening angles θ_c (in degrees) for the FRI (*left*) and the FRII (*right*) populations for the “Jet+Torus” model. For a given A_{V_0} , AIC was estimated at 2° intervals of θ_c . The shaded area denotes the region where the model becomes unphysical (see Sect. 3.5.1). In the physical regime, AIC reaches a minimum at around 90° for the FRIs and 37° for the FRIIs.

R_c region, is required to derive a more robust quantitative value for L_{disk} since at large R_c the jet overwhelms the disk emission and at very small R_c the torus obscures it. Table 2 lists the fitted parameters of the “Best fit” model for both the FR populations and Fig. 5 shows the best fit curves to each of the FR populations.

It is interesting here, that the “Jet-only” model is *unambiguously the best-fit for the FRIs*, whereas, *several models give comparable fits to the FRIIs*. Given this difference in the behaviour of the two classes, we carry the procedure a bit further by contrasting the behaviour of the AIC for the FRIs and FRIIs in the “Jet+Torus” model case. In Fig. 6 we plot the AIC against the torus half-opening angle for different fixed values of A_{V_0} . Figure 6 shows that the families of AIC plots for the two populations differ systematically from each other. The plots can be broadly divided into two parts. Below $\theta_c \approx 30^\circ$ the AIC drops for both the FRI and FRII population (shaded region in Fig. 6). This formally implies that the fit gets better for opening angles of the torus that are smaller than $\theta_c \approx 30^\circ$, but clearly is the result of the algorithm trying to fit the *entire* variation in L_0 by torus obscuration *alone*. For the FRIs,

above $\theta_c \approx 35^\circ$, the AIC declines again and reaches a minimum at angles close to 90° , consistent with there being no torus. For the FRIIs, on the other hand the AIC does not decline appreciably above $\theta_c \approx 35^\circ$. In addition it shows a conspicuous minimum at $\theta_c \approx 37^\circ$.

Thus although simple model-fitting using the LM algorithm yields ambiguous results for the FRIIs on the face of it, by rejecting the possibility of the entire variation in L_0 being due to obscuration by a torus we obtain model parameters that are broadly consistent with the predictions of the US. The model-fitting results in the best θ_c roughly coinciding with the angle where the upper limits to L_0 start appearing in FRII galaxies. The best A_{V_0} turns out to be ≈ 3 mag for the FRIIs at the best θ_c while for the FRIs, A_{V_0} turns out to be ≈ 0 . We point out that the A_{V_0} that we infer here is of the nature of a lower limit, since detection limits would exclude measured data points corresponding to higher values of A_{V_0} . We find that the behaviour of FRI and FRII optical nuclei is distinctly different in that the model-fitting results are unambiguous for the FRIs while they are not so for the FRIIs, hinting at intrinsic differences between FRIs and FRIIs.

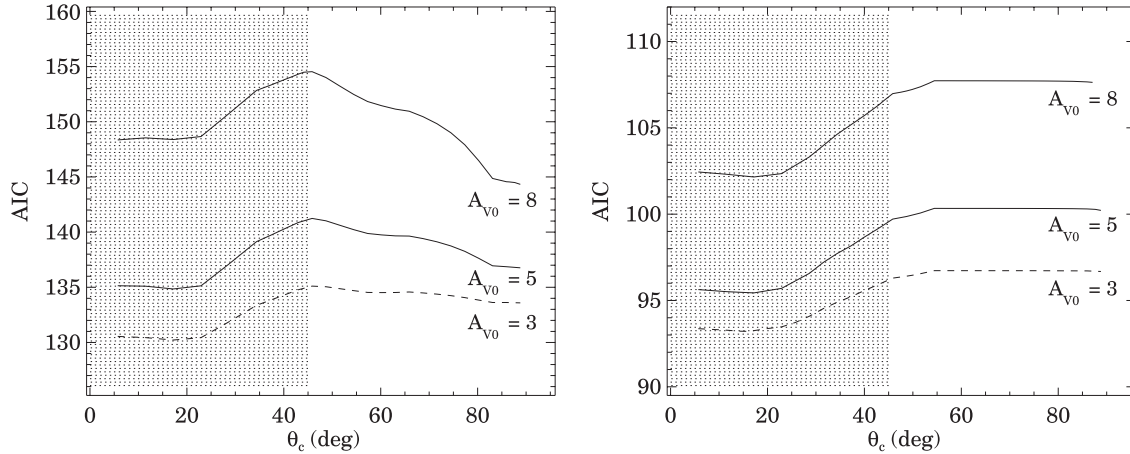


Fig. 7. AIC values for different initial A_{V_0} plotted against torus opening angles θ_c (in degrees) for the matched subsamples of FRI (*left*) and the FRII (*right*) populations for the “Jet+Torus” model. The shaded area denotes the region where the model becomes unphysical (see Sect. 3.5.1). In the physical regime, AIC reaches a minimum at around 90° for the FRIs while the case is not clear for the FRIIs.

It may be recalled that the BL Lac objects taken by themselves show a flatter logarithmic distribution of L_o against R_c than would be expected from beaming alone (Sect. 3.3), and indeed model fitting just the BL Lacs gives the “Jet+Disk” model to be the best one for them, with an implied L_{disk} of $3.3 \times 10^{22} \text{ WHz}^{-1}$ (see Table 2). As was stated in Sect. 3.3, this is most likely to be due to the contaminating host galaxy luminosity mimicking emission from a disk. We note however, that unless values for their optical nuclei are used that are uncontaminated by the host galaxy, we cannot totally rule out an accretion disk in the BL Lacs, and this implies that they may not be intrinsically similar to the FRI radio galaxies.

For the *smaller* matched subsamples of FRIs and FRIIs, the variation of AIC with θ_c (see Fig. 7) is broadly similar to that of their respective unrestricted samples. This validates our procedure and the *qualitative* results for the whole sample regarding the differences between the FRIs and FRIIs. The only discernible difference for the “matched” FRIIs is that the “AIC minimum” observed at $\theta_c \approx 37^\circ$ for the whole sample, is now no longer prominent. However, this may not be surprising in view of the fact that the “matched” FRII objects are much fewer in number, especially at low R_c values.

We note that for neither the FRIs nor FRIIs is there any correlation between the residuals of the model-fit with R_c and L_o . However, there seems to be a weak correlation for the BL Lacs considered alone. This may reflect the effects of ignoring the host galaxy luminosity when taking the nuclear optical luminosity.

We note that while reliable quantitative results cannot be obtained using the current data because of the drawbacks in the sample, the approach and the results indicate that it is a good approach to derive various parameters if data for a rigorous and large sample are available. Better data would allow more parameters to be incorporated and controlled.

3.5.2. The bulk Lorentz factor

As an approximation we assume that a single γ value is applicable to each population, and that all orientations are

represented in each population, and therefore that the minimum and maximum values of R_c in each population correspond to orientations perpendicular and parallel to our line of sight respectively. The formula using the R_c^{min} and R_c^{max} (Eq. (A.3) in the Appendix) results in the lower limit to the maximum Lorentz factor $\gamma_{\text{max}} \approx 9.7$ for the FRI population. For the FRII population we get a value of $\gamma_{\text{max}} \gtrsim 11.5$, obtained using a quasar with an upper limit to its extended radio emission, and therefore the actual lower limit to γ_{max} could be higher. These values broadly agree with those obtained by Urry & Padovani (1995): $\gamma_{\text{max}} \gtrsim 9$ for the FRI population and $\gtrsim 13$ for the FRII population assuming $p = 3$. However, based on the correlation of optical and radio core emission with the isotropic $\text{H}\alpha + [\text{NII}]$ emission, Verdoes Kleijn et al. (2002) have obtained a constraint on the value of γ of $\lesssim 2$ (assuming $p = 3$), albeit for FRI radio galaxies *alone*.

4. Conclusions

We use the radio core prominence R_c as a statistical indicator of orientation and find that the systematic differences between radio-loud AGN of the two Fanaroff-Riley types appear to also extend to their optical nuclei, in a manner that is consistent with the predictions of the simple US. We find that

1. The luminosity of the pc-scale optical nuclei in the FRI radio galaxies is orientation-dependent, while that in the FRII radio galaxies is not. This result is consistent with the idea that FRIIs contain an obscuring torus, (as required by the simple US) whereas there is no torus in the FRIs.
2. For the FRI radio galaxies, though the correlation with orientation is very significant, there remains considerable residual scatter. This may be due to obscuration from an *extended kpc-scale* dusty disk. The axis of this disk appears unrelated to the AGN axis. The residual scatter may also be due to intrinsic variation in the optical luminosity.
3. The nuclear optical luminosity correlates significantly with R_c , or, equivalently orientation, for the FRI radio galaxies and BL Lacs of FRI morphology taken

together – the FRI population. Our model-fitting suggests that a relativistically beamed optical jet gives the best fit.

4. For the FRII radio galaxies and radio-loud quasars taken together – the FRII population, the nuclear optical luminosity again correlates significantly with R_c . Our model-fitting indicates that formally the best fit is again a beamed synchrotron jet. But a beamed jet obscured by a torus with an inferred opening angle close to 40° is a comparable fit, and is able to explain the contrasting behaviour of the FRI and FRII data.
5. The scatter in the $L_o - R_c$ correlation for both the FR populations is likely to be primarily due to the spread in intrinsic AGN power, although extended dusty disks may also contribute to the scatter in FRI radio galaxies.
6. Our model-fitting suggests that the luminosity of the intrinsic (i.e., unbeamed) jet in the FRIIs is approximately an order of magnitude larger than for the FRIs, although this result needs to be confirmed using a rigorous sample.
7. The data for the broad-line FRIIs alone are fitted best by a model that comprises a relativistic jet and a geometrically thin optically thick disk, consistent with the presence of the “big blue bump” in them.

The robustness of the above results is limited by the facts that (a) the “samples” used are eclectic; (b) the luminosities of the optical nuclei in the highly beamed objects are contaminated by the contributions of the host galaxies; and (c) there could be variability between the epochs of the optical and radio measurements. A robust analysis requires rigorous measurement of the optical luminosity as well as samples that are rigorously selected, with the objects of a given FR population chosen to be intrinsically similar in the framework of the US and from the same volume of space.

Acknowledgements. We are very grateful to Prof. Thiriyambakam Krishnan for his scrutiny of our statistical tests and results, useful suggestions and extensive discussions. We also thank the anonymous referee for comments that improved the paper.

Appendix A: The model equations

We give here the equations that form the basis of our model-fitting procedure. In the most general case, we assume that the nuclear optical luminosity L_o is due to the sum of synchrotron emission from the base of a relativistic jet, and thermal emission from a thin accretion disk, modified by the presence of an optically thick torus. We write,

$$L_o = (\delta^p L_{\text{jet}}^{\text{int}} + L_{\text{disk}} \cos \theta) \times 10^{-A_V/2.5} \quad (\text{A.1})$$

$L_{\text{jet}}^{\text{int}}$ is the intrinsic synchrotron luminosity from the base of the jet which is relativistically beamed by the factor δ^p , where δ is the Doppler factor and for a jet spectral index of α the jet structure parameter p is given by $2+\alpha$ or $3+\alpha$ depending on whether the jet is continuous or blobby (e.g., Urry & Padovani 1995). L_{disk} is the luminosity of a geometrically thin optically thick accretion disk, whose apparent luminosity is orientation-dependent due to projection (the $\cos \theta$ term). A_V is the

extinction resulting from the torus in the V band. For a half-opening angle of the torus θ_c , we have,

$$A_V = A_{V_0} \left(1 - \frac{\cos \theta}{\cos \theta_c} \right) \quad \text{for } \theta \geq \theta_c \quad (\text{A.2})$$

$$A_V = 0 \quad \text{for } \theta < \theta_c$$

(Simpson 1996).

Thus, for $\theta = 90^\circ$ $A_V = A_{V_0}$.

For the Lorentz factor of bulk relativistic motion of the nuclear jet (e.g., Appendix C, Urry & Padovani 1995) we have,

$$\gamma = \left(\frac{1}{2^{p-1}} \frac{R_c^{\text{max}}}{R_c^{\text{min}}} \right)^{\frac{1}{2p}}, \quad (\text{A.3})$$

$$R_c^{\text{int}} = \frac{\gamma^p R_c^{\text{min}}}{2} \quad (\text{A.4})$$

where R_c^{min} and R_c^{max} are the minimum and maximum values of R_c , i.e., the values of R_c at edge-on ($\theta \sim 90^\circ$) and pole-on ($\theta \sim 0^\circ$) inclinations of the AGN respectively, and R_c^{int} is the intrinsic flux density ratio of the core and the extended radio emission. We now obtain the orientation to the line of sight, θ , in terms of R_c . We use the relativistic beaming formulae which take into account contributions from both the approaching and receding jet (e.g., Urry & Padovani 1995).

$$R_c = R_c^{\text{int}} \left[\frac{1}{[\gamma(1 - \beta \cos \theta)]^p} + \frac{1}{[\gamma(1 + \beta \cos \theta)]^p} \right]. \quad (\text{A.5})$$

We assume a value of 3 for the jet structure factor p . We note that Urry & Padovani (1995) infer a p value of ≈ 3 based on the observations of superluminal motion within our own galaxy by Mirabel & Rodriguez (1994). We get,

$$\beta \cos \theta = \left(1 - \frac{(2b)^{2/3}}{\sqrt{R_c}(-2\sqrt{R_c} + \sqrt{2b + 4R_c})^{1/3}} + \frac{(2b)^{1/3}(-2\sqrt{R_c} + \sqrt{2b + 4R_c})^{1/3}}{\sqrt{R_c}} \right)^{1/2} \quad (\text{A.6})$$

$$\text{where } b = \frac{R_c^{\text{int}}}{\gamma^p}.$$

Appendix B: The models and the fitting procedure

We describe here the model-fitting procedure and the use of the Akaike’s information criterion (AIC) to evaluate the models. We considered several simple models to compare the behaviour of the optical nuclei in the FRI and FRII populations. For the “Jet-only” model, the entire nuclear optical luminosity is ascribed to synchrotron emission from a jet which is relativistically beamed. For the “Jet+Disk” model, the nuclear optical luminosity is modelled as a combination of a beamed synchrotron jet and a thin optically thick disk. For the “Jet+Disk+Torus” model, Eq. (A.1) is used in toto. In the “Jet+Torus” model the entire nuclear optical luminosity is due to the beamed jet, modified by an obscuring torus.

Using the γ values derived as in Eq. (A.3) from the minimum and maximum values of R_c in our data set for each

of the FRI and FRII populations and Eqs. (A.1) and (A.5) for L_0 and R_c , we made a non-linear least squares fit to the data for both the FR populations separately. We used the Levenberg-Marquardt (LM) algorithm as implemented in the IDL package (the LMFIT routine). This routine gives the best-fit values of the free parameters, their standard deviations and the χ^2 goodness-of-fit. For the model-fitting we assumed the errors in the nuclear optical luminosity to be 50% (e.g., Verdoes Kleijn et al. 2002).

The Akaike's information criterion is used to compare different model-fits and is defined as

$$\text{AIC} = -2\ln(L) + 2k \quad (\text{B.1})$$

(Burnham & Anderson 2002),

where $\ln(L)$ is the log likelihood function and is given by

$$\ln(L) = -(n/2)\{\ln(2\pi) + \ln(\text{SEE}/n) + 1\} \quad (\text{B.2})$$

where “ n ” is the number of data-points, “SEE” is the Standard error of estimate and “ k ” is the number of parameters to be fitted. Smaller AIC values indicate a better fit. We note that the goodness-of-fit criterion AIC behaves in an inverse fashion to the χ^2 probability Q (Press et al. 1992).

For the “Jet-only” model, $L_{\text{jet}}^{\text{int}}$ is the only free parameter and the LM algorithm yields its best fit value. For the “Jet+Disk” model, both $L_{\text{jet}}^{\text{int}}$ and L_{disk} are free parameters. The output of the algorithm turned out to be independent of the input seed values of these free parameters. The “Jet+Disk+Torus” and the “Jet+Torus” models have two additional parameters of the torus, viz., A_{V_0} and θ_c . However, apart from the quality of the data, the fact that there is more than one “local minimum” for θ_c (discussed in Sect. 3.5.1) did not allow a robust estimation of all the parameters simultaneously. (The estimated values for θ_c strongly depended on the input seed value.) We therefore adopted the procedure of manually varying the extinction A_{V_0} and torus half-opening angle θ_c and using the resulting AIC for each pair of (fixed) A_{V_0} and θ_c to infer the best fit.

Considering first the most general “Jet+Disk+Torus” model to fit the data, we chose a range of values for the torus parameters, A_{V_0} and θ_c , and estimated the best fit $L_{\text{jet}}^{\text{int}}$ and L_{disk} using the LM algorithm. The results are tabulated in Table 2 for representative values, $A_{V_0} = 3$ and $\theta_c = 45^\circ$ (e.g., Barthel 1989). The resulting value of L_{disk} turned out to be insignificant in each case (see Table 2 and Sect. 3.5.1). We therefore further considered only the “Jet+Torus” model which seemed more applicable to the data. For a given value of A_{V_0} we varied the θ_c from 0° through 90° and tabulated the resultant AIC, which are plotted in Fig. 6.

As a next step, we fixed the torus half-opening angle θ_c to the value which had resulted in the minimum AIC (Fig. 6) – which is approximately the same for different values of A_{V_0} for each FR population, and let the A_{V_0} be the free parameter to be best-fitted by the LM algorithm. We found that the resultant A_{V_0} for the FRII objects was independent of the seed value whereas it depended on the initial value for the FRI objects. In this manner we estimated the “Best fit” “Jet+Torus” model with values of A_{V_0} and θ_c which gave the lowest AIC value.

References

- Akaike, H. 1974, IEEE Trans. Automatic Control, 19, 716
 Baker, J. C., Hunstead, R. W., Kapahi, V. K., & Subrahmanya, C. R. 1994, in The First Stromlo Symp.: The Physics of Active Galaxies, ed. G. V. Bicknell, M. A. Dopita, & P. J. Quinn, 195
 Barthel, P. D. 1989, ApJ, 336, 606
 Baum, S. A., Zirbel, E. L., & O’Dea, C. P. 1995, ApJ, 451, 88
 Becker, R. H., White, R. L., & Edwards, A. L. 1991, ApJS, 75, 1
 Blandford, R. D., & Konigl, A. 1979, ApJ, 232, 34
 Bridle, A. H., & Perley, R. A. 1984, ARA&A, 22, 319
 Burnham, K. P., & Anderson, D. R. 2002, Model selection and multimodel inference: a practical information-theoretic approach (New York, NY: Springer-Verlag)
 Capetti, A., & Celotti, A. 1999, MNRAS, 304, 434
 Capetti, A., Fanti, R., & Parma, P. 1995, A&A, 300, 643
 Capetti, A., Celotti, A., Chiaberge, M., et al. 2002, A&A, 383, 104
 Cassaro, P., Stanghellini, C., Bondi, M., et al. 1999, A&AS, 139, 601
 Chiaberge, M., Capetti, A., & Celotti, A. 1999, A&A, 349, 77
 Chiaberge, M., Capetti, A., & Celotti, A. 2000, A&A, 355, 873
 Chiaberge, M., Capetti, A., & Celotti, A. 2002, A&A, 394, 791
 de Koff, S., Best, P., Baum, S. A., et al. 2000, ApJS, 129, 33
 Falomo, R., Scarpa, R., & Bersanelli, M. 1994, ApJS, 93, 125
 Fanaroff, B. L., & Riley, J. M. 1974, MNRAS, 167, 31P
 Fomalont, E. B., & Bridle, A. H. 1978, AJ, 83, 725
 Giovannini, G., Feretti, L., Gregorini, L., & Parma, P. 1988, A&A, 199, 73
 Gregory, P. C., & Condon, J. J. 1991, ApJS, 75, 1011
 Hardcastle, M. J., Alexander, P., Pooley, G. G., & Riley, J. M. 1996, MNRAS, 278, 273
 Hardcastle, M. J., & Worrall, D. M. 1999, MNRAS, 309, 969
 Hardcastle, M. J., & Worrall, D. M. 2000, MNRAS, 314, 359
 Impey, C. D., & Tapia, S. 1990, ApJ, 354, 124
 Jannuzi, B. T., Yanny, B., & Impey, C. 1997, ApJ, 491, 146
 Jenkins, C. R. 1982, MNRAS, 200, 705
 Kapahi, V. K., & Saikia, D. J. 1982, J. A&A, 3, 465
 Kapahi, V. K., & Shastri, P. 1987, MNRAS, 224, 17P
 Kollgaard, R. I., Wardle, J. F. C., Roberts, D. H., & Gabuzda, D. C. 1992, AJ, 104, 1687
 Kotilainen, J. K., Falomo, R., & Scarpa, R. 1998, A&A, 336, 479
 Kuehr, H., Nauber, U., & Pauliny-Toth, I. I. K. 1979, A Catalogue of radio sources (Bonn: Max-Planck-Institut (MPI) für Radioastronomie)
 Kuehr, H., Pauliny-Toth, I. I. K., Witzel, A., & Schmidt, J. 1981, AJ, 86, 854
 Laing, R. A., Parma, P., de Ruiter, H. R., & Fanti, R. 1999, MNRAS, 306, 513
 Laurent-Muehleisen, S. A., Kollgaard, R. I., Moellenbrock, G. A., & Feigelson, E. D. 1993, AJ, 106, 875
 Laurent-Muehleisen, S. A., Kollgaard, R. I., Ryan, P. J., et al. 1997, A&AS, 122, 235
 Ledlow, M. J., & Owen, F. N. 1996, AJ, 112, 9
 Meier, D. L. 1999, ApJ, 522, 753
 Mirabel, I. F., & Rodriguez, L. F. 1994, Nature, 371, 46
 Morris, S. L., Stocke, J. T., Gioia, I. M., et al. 1991, ApJ, 380, 49
 O’Dea, C. P., Barvainis, R., & Challis, P. M. 1988, AJ, 96, 435
 Orr, M. J. L., & Browne, I. W. A. 1982, MNRAS, 200, 1067
 Padovani, P., & Giommi, P. 1995, MNRAS, 277, 1477
 Perlman, E. S., & Stocke, J. T. 1993, ApJ, 406, 430
 Perlman, E. S., Sparks, W. B., Radomski, J., et al. 2001, ApJ, 561, L51
 Pica, A. J., Smith, A. G., Webb, J. R., et al. 1988, AJ, 96, 1215
 Press, W. H., Flannery, B. P., Teukolsky, S. A., & Vetterling, W. T. 1992, Numerical Recipes in Fortran (Cambridge University Press)

- Prestage, R. M., & Peacock, J. A. 1988, *MNRAS*, 230, 131
- Rector, T. A., & Stocke, J. T. 2001, *AJ*, 122, 565
- Simpson, C. 1996, *Vistas Astron.*, 40, 57
- Slee, O. B., Siegman, B. C., & Perley, R. A. 1989, *Aust. J. Phys.*, 42, 633
- Smith, E. P., & Heckman, T. M. 1990, *ApJ*, 348, 38
- Spangler, S. R., & Sakurai, T. 1985, *ApJ*, 297, 84
- Urry, C. M., & Padovani, P. 1995, *PASP*, 107, 803
- Verdoes Kleijn, G. A., Baum, S. A., de Zeeuw, P. T., & O'Dea, C. P. 1999, *AJ*, 118, 2592
- Verdoes Kleijn, G. A., Baum, S. A., de Zeeuw, P. T., & O'Dea, C. P. 2002, *AJ*, 123, 1334
- Vermeulen, R. C., & Cohen, M. H. 1994, *ApJ*, 430, 467
- Véron-Cetty, M. P., & Véron, P. 1998, *VizieR Online Data Catalog*, 7207, 0
- Waggett, P. C., Warner, P. J., & Baldwin, J. E. 1977, *MNRAS*, 181, 465
- Webb, J. R., Smith, A. G., Leacock, R. J., et al. 1988, *AJ*, 95, 374
- Wills, B. J., Wills, D., Breger, M., Antonucci, R. R. J., & Barvainis, R. 1992, *ApJ*, 398, 454
- Xu, C., Baum, S. A., O'Dea, C. P., Wrobel, J. M., & Condon, J. J. 2000, *AJ*, 120, 2950
- Zirbel, E. L., & Baum, S. A. 1995, *ApJ*, 448, 521

Online Material

Appendix C: Data on sample objects

Table C.1. The FRI radio galaxies.

IAU name	Alternate name	Redshift z	b/a	$\log L_{\text{ext}}$ W Hz ⁻¹	$S_c(5 \text{ GHz})$ mJy	Ref.	$\log R_c$	$\log L_o$ W Hz ⁻¹	Ref.
0036+030	NGC 193	0.0144	0.18 ^d	22.60	40.0	6,15	-1.31	18.35	5
0053+261	3C 28	0.1952	...	25.42	<0.2	1,3	<-2.92	<19.48	1
0055-016	3C 29	0.0448	...	25.29	93.0	1,3	-1.39	19.43	1
0055+265	4C 26.03	0.0472	...	24.61	9.0	2	-1.93	<18.54	2
0055+300	NGC 315	0.0167	0.23 ^d	24.01	617.6	2	-0.39	19.19	5
0104+321	3C 31	0.0169	0.77 ^d	24.40	92.0	1,3	-1.34	19.08	5
0120+329	NGC 507	0.0164	...	22.29	1.5	2	-1.30	<17.64	2
0123-016	3C 40	0.0180	0.91 ^d	22.17	67.8	10	-1.64	<18.63	5
0153+053	NGC 741	0.0185	...	22.75	6.0	11	-1.65	<18.35	5
0220+427	3C 66B	0.0215	0.98 ^d	24.86	182.0	1,3	-1.29	19.62	5
0305+039	3C 78	0.0288	...	24.96	964.0	1,3	-0.42	20.66	1
0318+415	3C 83.1	0.0251	0.09 ^d	24.98	21.0	1,3	-2.22	18.31	1
0316+413	3C 84	0.0176	...	24.73	42370.0	1,3	1.02	21.03	1
0331-013	3C 89	0.1386	...	25.80	49.0	1,3	-1.21	<18.97	1
0705+486	NGC 2329	0.0193	0.68 ^d	23.02	69.0	11	-0.44	20.04	5
0755+379	3C 189	0.0413	...	24.43	228.8	2	-0.46	20.18	2
0924+301	...	0.0266	...	23.52	0.4	2	<-2.64	<17.98	2
0928+678	NGC 2892	0.0225	...	22.82	30.0	12	-0.52	19.15	5
1142+198	3C 264	0.0206	0.99 ^d	24.57	200.0	1,3	-1.00	20.15	5
1205+255	UGC 7115	0.0226	...	22.58	44.0	11	-0.51	19.48	5
1216+061	3C 270	0.0074	0.46 ^d	24.31	308.0	1,3	-1.44	17.56	5
1220+587	NGC 4335	0.0154	0.41 ^d	22.64	15.0	6	-0.44	<19.01	5
1222+131	3C 272.1	0.0037	0.15 ^l	23.22	180.0	1,3	-1.18	18.17	5
1228+126	3C 274	0.0037	...	24.63	4000.0	1,3	-1.24	19.18	5
1257+282	NGC 4874	0.0239	...	23.07	1.2	2	-1.87	<17.49	2
1322+366	NGC 5141	0.0173	0.25 ^l	23.63	78.7	10	-0.61	<18.69	5
1336+391	3C 288	0.2460	...	26.42	30.0	1,3	-1.56	20.03	1
1346+268	4C 26.42	0.0633	...	24.52	59.3	2	-0.78	19.58	2
1407+177	NGC 5490	0.0162	0.35 ^l	23.24	37.8	10	-1.28	<17.48	5
1414+110	3C 296	0.0237	0.29 ^d	24.61	77.0	1,3	-1.33	18.64	1
1422+268	...	0.0370	...	23.99	21.1	2	-1.15	<19.41	2
1430+251	4C 25.46	0.0813	...	24.20	1.2	2	<-1.93	<19.61	2
1450+281	...	0.1265	...	24.48	6.7	2	-1.12	<19.77	2
1502+261	3C 310	0.0540	...	25.19	80.0	1,3	-1.19	19.38	1
1510+709	3C 314.1	0.1197	...	25.33	<1.0	1,3	<-2.55	<19.52	1
1514+072	3C 317	0.0342	...	24.43	391.0	1,3	-0.13	19.49	1
1521+288	4C 28.39	0.0825	...	24.53	55.8	2	-0.60	20.20	2
1527+308	...	0.1143	...	24.03	4.0	2	-0.97	<19.89	2
1553+245	...	0.0426	...	23.43	57.9	2	-0.03	19.84	2
1610+296	NGC 6086	0.0313	...	22.92	1.1	2	<-1.52	<18.38	2
1613+275	...	0.0647	...	24.01	10.6	2	-1.00	<19.24	2
1626+396	3C 338	0.0303	...	24.19	105.0	1,3	-0.57	19.33	1
1637+826	NGC 6251	0.024	...	23.82	720.0	13,4	0.44	20.19	7
1641+173	3C 346	0.1620	...	26.20	220.0	1,3	-0.82	21.17	1
1648+050	3C 348	0.1540	...	27.12	10.0	1,3	-3.13	19.67	1
1827+323	...	0.0659	...	24.04	20.8	2	-0.71	<19.38	2
2045+068	3C 424	0.1270	...	25.67	18.0	1,3	-1.58	<19.77	1
2116+262	NGC 7052	0.0164	0.30 ^d	22.97	47.0	9,14	-0.22	18.26	8
2153+377	3C 438	0.2900	...	26.77	17.0	1,3	-2.02	<19.94	1
2212+135	3C 442	0.0262	...	24.39	2.0	1,3	-2.61	18.16	1
2229+391	3C 449	0.0181	0.50 ^d	24.29	37.0	1,3	-1.56	19.13	1
2236+350	UGC 12127	0.0277	...	23.46	7.1	2	-1.34	18.55	2
2318+079	NGC 7626	0.0113	0.17 ^l	22.39	15.6	10	-1.47	<17.91	5
2335+267	3C 465	0.0301	0.69 ^l	25.00	270.0	1,3	-0.97	19.60	1

Superscripts “*d*” and “*l*” for b/a stand for extended dust disks and lanes, respectively. References: (1): Chiaberge et al. (1999) (*F702W* filter); For the 7 sources which were common between the 3CR, B2 and the UGC samples we used the *F555W* flux densities from Verdoes Kleijn et al. (2002); (2): Capetti et al. (2002) (1.4 GHz, *F814W* filter); (3): Kuehr et al. (1979) (5 GHz); (4): Kuehr et al. (1981) (5 GHz); (5): Verdoes Kleijn et al. (2002) (*F555W* filter); (6): Xu et al. (2000) (1.4 GHz); (7): Hardcastle & Worrall (1999) (*F702W* filter); (8): (Capetti & Celotti 1999) (*F814W* filter); (9): Giovannini et al. (1988) (5 GHz); (10): Bridle & Perley (1984) (core at 5 GHz, total flux density at 1.4 GHz); (11): Laurent-Muehleisen et al. (1997) (5 GHz); (12): Jenkins (1982) (5 GHz); (13): Waggett et al. (1977) (2.7 GHz); (14): Gregory & Condon (1991) (5 GHz); (15): Becker et al. (1991) (5 GHz).

Table C.2. The FRII radio galaxies.

IAU name	Alternate name	Redshift z	b/a	$\log L_{\text{ext}}$ W Hz ⁻¹	$S_c(5 \text{ GHz})$ mJy	Ref.	$\log R_c$	$\log L_o$ W Hz ⁻¹	Ref.
0034-014	3C 15	0.073	...	25.46	372.8	1,3	-0.52	<19.74	1
0035-024	3C 17*	0.220	...	26.63	727.9	1,3	-0.48	21.64	1
0038+097	3C 18	0.188	...	26.41	118.2	1,3	-1.18	21.36	1
0106+729	3C 33.1*	0.181	...	26.11	19.7	1,3	-1.69	20.94	1
0109+492	3C 35	0.067	...	25.06	23.7	1,3	-1.40	<19.31	1
0218-021	3C 63	0.175	...	26.10	18.3	1,3	-1.74	21.04	1
0307+169	3C 79	0.256	...	26.62	14.7	1,3	-2.03	21.02	1
0325+023	3C 88	0.030	...	24.86	197.2	1,3	-0.97	19.46	1
0356+102	3C 98	0.030	...	25.25	11.1	1,3	-2.61	<18.53	1
0415+379	3C 111*	0.049	...	25.86	1155.3	1,4	-0.77	20.99	1
0433+295	3C 123	0.218	...	27.55	85.0	1,3	-2.33	<19.16	1
0453+227	3C 132	0.214	...	26.35	33.5	1,3	-1.56	<19.55	1
0459+252	3C 133	0.277	...	26.85	170.8	1,3	-1.14	20.68	1
0511+008	3C 135	0.127	...	25.88	5.5	1,3	-2.31	20.15	1
0605+480	3C 153	0.277	...	26.68	0.4	1,3	-3.56	<19.34	1
0640+233	3C 165	0.296	...	26.48	8.7	1,3	-2.01	19.95	1
0642+214	3C 166	0.245	...	26.15	553.6	1,3	-0.03	20.71	1
0651+542	3C 171	0.238	...	26.49	2.5	1,3	-2.74	19.20	1
0734+805	3C 184.1	0.118	...	25.87	7.5	1,3	-2.23	20.96	1
0802+243	3C 192	0.060	...	25.56	8.5	1,3	-2.44	<19.94	1
0818+472	3C 197.1	0.131	...	25.82	6.8	1,3	-2.13	20.88	1
0819+061	3C 198	0.082	...	25.14	<1.5	5,4	<-2.50	20.85	1
0917+458	3C 219*	0.174	...	26.49	68.7	1,3	-1.56	21.39	1
0936+361	3C 223	0.137	...	26.04	11.7	1,3	-2.07	<20.05	1
0938+399	3C 223.1	0.108	...	25.65	8.7	1,3	-2.02	<19.98	1
0945+076	3C 227*	0.086	...	25.94	23.5	1,3	-2.07	21.66	1
0958+290	3C 234*	0.185	...	26.34	133.6	1,3	-1.07	21.85	1
1003+351	3C 236	0.099	...	25.70	191.5	1,3	-0.80	<19.84	1
1205+341	...	0.0788	...	24.46	12.5	2	-1.21	<19.81	2
1251+278	3C 277.3	0.0857	...	25.37	12.4	2	-2.05	19.49	2
1319+428	3C 285	0.079	...	25.32	7.8	1,3	-2.00	18.47	1
1330+022	3C 287.1*	0.216	...	26.34	443.8	1,3	-0.42	21.43	1
1420+198	3C 300	0.270	...	26.58	10.1	1,3	-2.12	20.47	1
1441+522	3C 303*	0.141	...	25.83	187.6	1,3	-0.64	21.44	1
1519+078	3C 318.1	0.046	...	24.49	3.0	6,3	-2.05	<18.52	1
1522+546	3C 319	0.192	...	26.04	1.4	1,3	-2.72	<20.14	1
1545+210	3C 323.1*	0.264	...	26.44	43.8	1,3	-1.36	22.83	1
1549+202	3C 326	0.089	0.24 ^d	25.19	15.9	1,3	-1.46	<19.91	1
1559+021	3C 327	0.104	...	26.18	40.8	1,3	-1.91	<19.35	1
1615+325	3C 332*	0.152	...	25.93	11.5	1,3	-1.89	21.56	1
1658+471	3C 349	0.205	...	26.33	21.9	1,3	-1.76	20.88	1
1717-009	3C 353	0.030	...	25.94	216.2	1,3	-2.01	<18.40	1
1726+318	3C 357	0.167	...	26.10	6.5	1,3	-2.23	<19.66	1
1825+743	3C 379.1	0.256	...	26.32	3.9	7,3	-2.32	<19.91	1
1832+474	3C 381	0.161	...	26.18	6.9	1,3	-2.31	<20.28	1
1833+326	3C 382*	0.058	...	25.47	228.1	1,4	-0.95	22.56	1
1842+455	3C 388	0.091	...	25.80	76.5	1,3	-1.37	20.07	1
1845+797	3C 390.3*	0.056	...	25.74	434.7	1,3	-0.97	21.88	1
1939+605	3C 401	0.201	...	26.41	47.5	1,3	-1.52	20.35	1
1940+505	3C 402	0.025	...	24.39	48.1	1,3	-1.27	19.46	1
1949+023	3C 403	0.059	...	25.54	12.1	1,3	-2.28	19.49	1
2221-023	3C 445*	0.057	...	25.40	382.8	1,3	-0.66	22.11	1
2243+394	3C 452	0.081	0.27 ^l	25.96	152.3	1,3	-1.33	<19.72	1
2309+090	3C 456	0.233	...	26.24	27.8	1,3	-1.45	21.21	1
2318+235	3C 460	0.268	...	26.02	21.4	1,4	-1.24	20.29	1

Superscripts “*d*” and “*l*” for b/a stand for extended dust disks and lanes, respectively. There are only two FRIIs for which b/a for extended dust features are available (de Koff et al. 2000). We do not include the FRIIs in our analysis of the extended dusty disks. Sources with a star are BLRGs. References: (1): Chiaberge et al. (2002) (5 GHz, *F702W* filter, except 3C 192 observed with *F555W*); (2): Capetti et al. (2002) (1.4 GHz); (3): Kuehr et al. (1979) (5 GHz); (4): Véron-Cetty & Véron (1998) (5 GHz); (5): Fomalont & Bridle (1978) (5 GHz); (6): Slee et al. (1989) (1.5 GHz); (7): Spangler & Sakurai (1985) (1.4 GHz).

Table C.3. The BL Lac objects.

IAU name	Alternate name	Redshift z	m_v	Ref.	$\log L_{\text{ext}}$ W Hz ⁻¹	$S_c(5 \text{ GHz})$ mJy	Ref.	$\log R_c$	$\log L_o$ W Hz ⁻¹
0158+003	...	0.299	17.96	1	24.36	8.38	2	0.60	22.61
0219-164	...	0.698	17.0	9	25.50	358.0	5	0.84	23.78
0219+428	3C 66A	0.444	15.08	6	27.32	814.0	2 ^a	0.14	24.13
0257+344	...	0.247	18.53	1	23.22	11.78	2	1.69	22.21
0317+185	...	0.190	18.12	1	23.50	9.85	2	1.08	22.13
0323+022	...	0.147	16.98	6	23.20	55.0	5	1.21	22.36
0414+009	...	0.287	17.11	6	24.50	67.0	5	0.54	22.91
0454+844	...	1.34*	17.3	9	24.21	1400.0	4	>3.37 [†]	24.29
0521-365	...	0.055	14.62	9	26.12	3124.0	2 ^a	-0.14	22.43
0548-322	...	0.069	16.05	8	24.67	80.0	2 ^a	-0.08	22.06
0607+711	...	0.267	19.60	1	24.79	14.08	2	0.29	21.85
0706+592	...	0.124	18.40	9	24.20	65.0	5	0.17	21.64
0735+178	...	>0.424	15.40	9	23.82	1990.0	4	>3.2	23.96
0737+746	...	0.315	16.89	1	23.85	24.47	2	1.64	23.09
0851+202	OJ287	0.306	13.81	7	24.21	2217.0	2 ^a	3.23	24.29
1101-232	...	0.186	17.01	8	24.40	49.0	5	0.41	22.56
1101+384	Mrk 421	0.030	13.22	6	23.85	520.0	2 ^a	0.81	22.46
1133+704	Mrk 180	0.044	14.49	9	24.31	131.0	2 ^a	0.09	22.29
1218+304	...	0.130	15.80	6	22.79	62.0	5	>1.34	22.72
1219+285	ON 231	0.102	15.40	7	23.07	2058.0	2 ^a	3.25	22.67
1221+248	...	0.218	17.65	1	23.64	27.85	2	1.53	22.45
1229+645	...	0.164	16.89	1	23.73	42.49	2	1.34	22.49
1235+632	...	0.297	18.59	1	24.00	13.0	5	>0.32	22.35
1400+162	...	0.244	16.74	9	26.27	233.0	2 ^a	-0.07	22.91
1402+042	...	0.344	16.88	8	24.40	21.43	2	0.53	23.17
1407+599	...	0.495	19.67	1	25.76	14.12	2	0.08	22.39
1418+546	...	0.152	15.39	6	24.31	1058.0	2 ^a	2.09	23.03
1426+427	...	0.130	16.40	9	23.50	31.0	5	>1.04	22.48
1443+638	...	0.299	19.65	1	24.63	8.36	2	0.33	21.93
1458+228	...	0.235	16.79	1	23.98	29.0	2	1.28	22.86
1514-241	AP Lib	0.049	14.97	7	23.61	2562.0	2 ^a	2.18	22.19
1534+018	...	0.312	18.70	1	25.28	28.84	2	0.26	22.35
1538+149	4C 14.60	0.605	17.89	6	26.94	1337.0	2 ^a	1.17	23.29
1552+203	...	0.222	17.70	1	24.65	33.09	2	0.61	22.44
1652+398	Mrk501	0.034	14.08	6	23.52	1376.0	2 ^a	1.66	22.23
1727+502	...	0.055	16.12	6	23.83	175.0	2 ^a	0.89	21.83
1749+096	...	0.320	17.32	6	23.89	744.0	2 ^a	>3.11	22.93
1807+698	3C 371	0.050	14.57	7	25.04	1350.0	2 ^a	0.48	22.37
2143+070	...	0.237	18.04	1	24.99	44.63	2	0.46	22.37
2155-304	...	0.117	13.31	6	25.18	252.00	2 ^a	0.37	23.62
2200+420	BL Lac	0.069	15.42	7	23.93	3310.00	2 ^a	2.26	22.31
2201+044	...	0.028	15.47	8	23.70	316.00	5	0.25	21.50
2254+074	...	0.190	16.29	6	24.51	454.00	2 ^a	1.73	22.87
2356-309	...	0.165	17.18	8	23.50	42.00	5	0.90	22.38

Redshift with a star is from Rector & Stocke (2001) – $\log R_c$ [†] was thus calculated for this new z using the $\log R_c$ quoted in Vermeulen & Cohen (1994). References: (1): Morris et al. (1991); (2): Perlman & Stocke (1993) (*EMSS* XBLs except 2^a which are RBLs, 1.4 GHz); (4): $\log R_c$ from Vermeulen & Cohen (1994); (5): Laurent-Muehleisen et al. (1993) (*HEAO-1* XBLs, 1.5 GHz); (6): Pica et al. (1988); (7): Webb et al. (1988); (8): Falomo et al. (1994); (9): Padovani & Giommi (1995).

Table C.4. The Radio-loud quasars.

IAU name	Alternate name	Redshift z	m_v	Ref.	$\log L_{\text{ext}}$ W Hz $^{-1}$	$S_c(5 \text{ GHz})$ mJy	Ref.	$\log R_c$	$\log L_o$ W Hz $^{-1}$
0016+731	...	1.781	19.00	4	27.37	>1500.0	1	>0.7	23.88
0106+013	...	2.107	18.39	4	27.65	3470.0	1	0.9	24.29
0153+744	...	2.338	16.00	4	26.26	1510.0	1	>2.0	25.35
0212+735	...	2.367	20.00	4	25.03	2200.0	1	>3.4	23.76
0234+285	...	1.207	18.50	4	25.68	1440.0	1	2.1	23.71
0333+321	NRAO140	1.259	17.50	4	26.44	2460.0	1	1.6	24.15
0458-020	...	2.286	19.50	4	27.17	1600.0	1	1.1	23.93
0615+820	...	0.710	17.50	4	26.38	>900.0	1	>0.8	23.60
0711+356	...	1.620	19.00	4	25.96	1500.0	1	>2.1	23.79
0723+679	3C 179	0.846	18.00	4	27.54	320.0	1	-0.68	23.57
0835+580	3C 205	1.536	17.62	4	27.89	23.0	1	-1.74	24.29
0836+710	...	2.180	16.50	4	27.04	2550.0	1	1.4	25.08
0839+616	...	0.862	17.85	4	26.84	34.0	1	-0.94	23.64
0850+581	...	1.322	18.00	4	27.45	1090.0	1	0.27	23.99
0906+430	3C 216	0.670	18.10	4	27.21	1060.0	1	-0.01	23.30
0923+392	4C 39.25	0.698	17.86	4	26.77	7320.0	1	1.3	23.44
1039+811	...	1.260	16.50	4	26.20	1120.0	1	1.5	24.55
1040+123	3C 245	1.028	17.29	4	27.44	860.0	1	0.0	24.04
1150+812	...	1.250	18.50	4	26.50	1140.0	1	1.2	23.74
1156+295	...	0.729	14.41	4	26.32	810.0	1	0.83	24.86
1222+216	4C 21.35	0.435	17.50	4	26.47	420.0	1	-0.01	23.14
1226+023	3C 273	0.158	12.85	4	26.70	39000.0	1	0.9	24.08
1253-055	3C 279	0.538	17.75	4	27.07	14500.0	1	1.1	23.24
1458+718	3C 309.1	0.905	16.78	4	27.63	2680.0	1	0.2	24.12
1641+399	3C 345	0.594	15.96	4	26.33	5520.0	1	1.5	24.05
1642+690	...	0.751	20.50	4	26.67	1260.0	1	0.7	22.45
1721+343	4C 34.47	0.206	15.46	4	25.95	470.0	1	-0.05	23.27
1828+487	3C 380	0.691	16.81	4	27.32	6590.0	1	0.7	23.85
1830+285	4C 28.45	0.594	17.16	4	27.02	450.0	1	-0.28	23.57
1901+319	3C 395	0.635	17.50	4	26.81	1480.0	1	0.5	23.49
1928+738	...	0.302	16.06	4	25.75	3210.0	1	1.3	23.38
1951+498	...	0.466	17.50	4	26.09	91.0	1	-0.24	23.20
2223-052	3C 446	1.404	18.39	4	28.24	2310.0	1	-0.15	23.90
2251+158	3C 454.3	0.859	16.10	4	27.05	9690.0	1	1.3	24.34

References: (1): $\log R_c$ from Vermeulen & Cohen (1994); (4): Véron-Cetty & Véron (1998).